ARTICLE IN PRESS

Cell Death Discovery

https://doi.org/10.1038/s41420-026-03022-0

Article in Press

Mitochondrial IκBα fuels cancer progression through metabolic rewiring, endothelial activation, and thrombotic spread

Received: 25 November 2025

Revised: 29 January 2026

Accepted: 5 March 2026

Cite this article as: Alessio, M., Petiti, J., Basile, R. *et al.* Mitochondrial IκBα fuels cancer progression through metabolic rewiring, endothelial activation, and thrombotic spread. *Cell Death Discov.* (2026). https://doi.org/10.1038/s41420-026-03022-0

Menga Alessio, Jessica Petiti, Roberta Basile, Pietro Poggio, Davide Acquarone, Alfonso Scalera, Lidia Avalle, Francesca Orso, Alessandra Bertoni, Paolo Ettore Porporato, Chiara Riganti, Lukasz Truszkowski, Isaia Barbieri, Mara Brancaccio, Carla Riera Domingo, Federica Cappellesso, Chiara Donno, Maiara Caroline Colombera, Massimiliano Mazzone, Giovanna Carrà & Alessandro Morotti

We are providing an unedited version of this manuscript to give early access to its findings. Before final publication, the manuscript will undergo further editing. Please note there may be errors present which affect the content, and all legal disclaimers apply.

If this paper is publishing under a Transparent Peer Review model then Peer Review reports will publish with the final article.

ARTICLE IN PRESS

© The Author(s) 2026. **Open Access** This article is licensed under a Creative Commons Attribution 4.0 International License, which permits use, sharing, adaptation, distribution and reproduction in any medium or format, as long as you give appropriate credit to the original author(s) and the source, provide a link to the Creative Commons licence, and indicate if changes were made. The images or other third party material in this article are included in the article's Creative Commons licence, unless indicated otherwise in a credit line to the material. If material is not included in the article's Creative Commons licence and your intended use is not permitted by statutory regulation or exceeds the permitted use, you will need to obtain permission directly from the copyright holder. To view a copy of this licence, visit http://creativecommons.org/licenses/by/4.0/.

ARTICLE IN PRESS

Mitochondrial IκBα Fuels Cancer Progression Through Metabolic Rewiring, Endothelial Activation, and Thrombotic Spread

Alessio Menga[1], Jessica Petiti[2], Roberta Basile[1], Pietro Poggio[3], Davide Acquarone[3], Alfonso Scalera[3], Lidia Avalle[4], Francesca Orso[5], Alessandra Bertoni[5], Paolo Ettore Porporato[3], Chiara Riganti[6], Lukasz Truszkowski[3], Isaia Barbieri[3], Mara Brancaccio[3], Carla Riera Domingo[7,8], Federica Cappellesso[9], Chiara Donno[1], Maiara Caroline Colombera[3], Massimiliano Mazzone[7,8], Giovanna Carrà[10,11*], Alessandro Morotti[10,11*].

1-University of Eastern Piedmont, Department of Health Sciences - Center for translational Research on Autoimmune & Allergic Diseases - CAAD Corso Trieste 15/A, 28100 Novara - Italy
2-Division of Advanced Materials Metrology and Life Sciences, Istituto Nazionale di Ricerca Metrologica (INRiM), 10135 Turin, Italy
3-Department of Molecular Biotechnology and Health Sciences-Molecular Biotechnology Center "Guido Tarone", University of Turin, Via Nizza 52, 10126 Turin, Italy;
4-Department of Science and Technological Innovation (DISIT), University of Eastern Piedmont, 15121 Alessandria, Italy.
5-Department of Translational Medicine (DIMET), University of Eastern Piedmont, Via Solaroli 17, Novara, 28100, Italy.
6-Department of Oncology, University of Torino, via Nizza 44, 10126, Torino, Italy; Molecular Biotechnology Center. Interdepartmental Center "G.Scansetti" for the study of asbestos and other toxic particulates, University of Torino, 10126 Torino, Italy.
7-Laboratory of Tumor Inflammation and Angiogenesis, Center for Cancer Biology, VIB, Leuven, Herestraat 49/bus 912, 3001, Belgium.
8-Laboratory of Tumor Inflammation and Angiogenesis, Department of Oncology, Center for Cancer Biology, Herestraat 49/bus 912, 3001 Leuven, Belgium.
9-Brussels center for Immunology, Vrije Universiteit Brussels, Brussels, Belgium
Lab of Dendritic Cell Biology and Cancer Immunotherapy, VIB Center for Inflammation Research, Pleinlaan 2 1050 Brussels, Belgium.
10-San Luigi Gonzaga Hospital, Regione Gonzole 10043, Orbassano, Italy;
11-Department of Clinical and Biological Sciences, University of Turin, Italy;

* These authors contributed equally

Correspondence: Giovanna Carrà PhD Department of Clinical and Biological Sciences, University of Turin, Italy; San Luigi Gonzaga Hospital, Orbassano, Italy. Biotechnology Center "Guido Tarone", University of Turin, Via Nizza 52, 10126 Turin, Italy. giovanna.carra@unito.it; Alessandro Morotti PhD, MD Department of Clinical and Biological Sciences, University of Turin, Italy; San Luigi Gonzaga Hospital, Orbassano, Italy. alessandro.morotti@unito.it;

ARTICLE IN PRESS

ARTICLE IN PRESS

Keywords: lung cancer, metastases, Mitochondria, Endothelial Cells, Thrombosis IκBα.

Abstract: Mitochondria play a central role in metastatic spread and cancer progression, with the IκBα/NF-κB signaling axis acting as a key regulator of both processes. We suggest that a stable fraction of IκBα localizes to mitochondria, where it escapes proteasomal degradation and acquires oncogenic functions independent of its canonical role in NF-κB inhibition. Using engineered A549 lung cancer cells with enforced mitochondrial localization of IκBα (IκBα-MTS), we show that the IκBα mitochondrial pool promotes increased cell proliferation, enhanced migration, and resistance to chemotherapy-induced apoptosis, along with a metabolic reprogramming characterized by elevated glycolysis and lactate secretion. These changes activated endothelial cells (ECs) and triggered cancer-associated thrombosis (CAT). This prothrombotic state, marked by elevated vWF a potent trigger for platelet adhesion and activation, contributed to an environment favorable for metastatic dissemination.

Our findings reveal mitochondrial IκBα as a key mediator in mitochondrial stress, endothelial activation, and thrombo-inflammatory mechanisms that drive lung cancer progression.

ARTICLE IN PRESS

ARTICLE IN PRESS

INTRODUCTION

Metastasis remains the primary cause of cancer-related mortality and is no longer viewed as a process solely driven by intrinsic properties of cancer cells[1,2]. Instead, successful metastatic colonization requires a coordinated remodeling of both the tumor and its microenvironment, including immune reprogramming, endothelial activation, and the establishment of a permissive vascular niche [3–5].

Central to this interplay is the metabolic plasticity of cancer cells, which not only sustains their growth but also actively reshapes the tumor microenvironment (TME). Metabolic rewiring, particularly the shift toward aerobic glycolysis (Warburg effect), leads to the production of lactate and other oncometabolites that contribute to immune evasion, angiogenesis, and matrix remodeling [6–8]. More recently, cancer metabolism has also been implicated in coagulopathy and thrombosis, phenomena collectively referred to as cancer-associated thrombosis (CAT) [9,10]. The resulting prothrombotic state facilitates tumor cell adhesion, immune evasion, and dissemination, thus linking metabolism directly to metastatic potential [11].

Within this context, the NF-κB signaling axis and, in particular, its inhibitor IκBα, emerges as a multifaceted regulator of cancer cell fate. Classically known for its role in inflammation and immune responses, IκBα inhibits NF-κB by sequestering it in the cytoplasm under basal conditions, preventing its transcriptional activity. Interestingly, IκBα also exhibits unexpected mitochondrial localization and functions [12–17]. In several cancer models, including lung cancer, IκBα is enriched at the outer mitochondrial membrane (OMM), where it can modulate apoptotic signaling. Its mitochondrial accumulation is further influenced by hypoxic conditions, a hallmark of rapidly growing tumors. Despite increasing recognition of mitochondrial IκBα, its role in cancer cell metabolism and metastatic behavior remains poorly understood. We have recently shown that alterations in mitochondrial IκBα not only affect apoptotic thresholds but also drive metabolic dysfunction, leading to lactate accumulation and endothelial activation [18]. These changes are closely linked to the release of von Willebrand factor (vWF), a prothrombotic glycoprotein that contributes to endothelial permeability, inflammation, and ultimately cancer cell extravasation [19–25]. Emerging evidence suggests that thrombosis is not merely a complication of advanced malignancy but an active driver of metastasis formation [22,26]. Tumor-induced endothelial activation and vWF release contribute to a self-reinforcing loop of vascular inflammation, coagulation, and metastatic seeding. In this study, we investigate the role of mitochondrial IκBα in

ARTICLE IN PRESS

orchestrating these events by integrating metabolic rewiring, prothrombotic signaling, and vascular remodeling. Our findings reveal a novel axis whereby mitochondrial IκBα enhances lung cancer cell aggressiveness through the promotion of a hypercoagulable, pro-metastatic microenvironment. This underscores a previously unrecognized link between mitochondrial signaling, cancer metabolism, and endothelial dysfunction in the pathogenesis of lung cancer metastasis.

MATERIAL AND METHODS

Cell lines

The human lung cancer cell lines A549 (RRID: CVCL_0023) and H460 (RRID: CVCL_0459) were purchased from ATCC. The cells were cultured in RPMI 1640 medium supplemented with 10% FBS, 1% L-glutamine, and 1% penicillin/streptomycin. All cell lines were maintained in a humidified incubator with 5% CO_2 at 37 °C. HUVECs, sourced from pooled donors, were acquired from PromoCell (Cat.No.C-12205) and cultivated in dishes coated with 0.2% gelatin, utilizing Endothelial Cell Growth Medium 2 (EGM2) enriched with provided growth factors (PromoCell, C-22011), penicillin (100 U/ml), and streptomycin (100 µg/ml; Gibco). HUVECs were utilized between passages 3 and 7, with medium renewal occurring every 48 or 72 hours. The cells were routinely tested and confirmed to be free of mycoplasma and bacterial contamination.

Cell proliferation assay and apoptosis assessment

For the cell proliferation assay, cells were plated in 96-well plates at a density of 2 × 10^3 cells per well. Proliferation was measured using the CellTiter-Glo assay (Promega). Apoptosis was assessed by flow cytometry after Annexin V staining (Biolegend, #640920). Data acquisition and analysis were performed using a FACSCelesta cytometer and CellQuest software. Both assays were performed according to the manufacturers' instructions.

MitoTracker

For MitoTracker staining (Invitrogen, #M7510), cells were seeded at a confluence of 2.5 × 10^5 cells per well in 6-well plates. MitoTracker was then added to the culture medium at a final concentration of 10 nM and incubated for 15 minutes at 37 °C. Subsequently, cells were evaluated by immunofluorescence.

Elyra 7 Structured Illumination Microscope

A549 cells (50 × 10^3 cells) were cultured in 24-well plates. Cells were imaged on the Elyra 7 Structured Illumination Microscope (Zeiss) in SIM mode, using a 100x oil-

ARTICLE IN PRESS

immersion objective and acquiring Z-stacks with a Z-step of 100 nm, covering the entire cell. The images were then processed using ZEN Black software (Zeiss) with SIM2 script (3D-leap mode, default settings for fixed samples; IκBα protein – weak signal settings, mitochondria – strong signal settings).

Wound-healing assay

A549 and H460 cells infected with lentivirus carrying either IκBα-WT, IκBα-MTS, or a control were seeded in 6-well plates and cultured until reaching 90% confluence. Subsequently, the cells were starved for 24 hours. After starvation, a wound was created in the center of the cell monolayer using a sterile plastic pipette tip. Serum-free medium was added to each well, and images of the wounds were captured at time 0 and after 15 hours using live-cell imaging microscopy (Carl Zeiss). The percentage of wound closure was quantified using either the Axio Vision program or ImageJ with the Wound-Healing Size Tool.

Anchorage-independent cell growth

Anchorage-independent cell-growth assays were conducted by suspending cells in 0.45% type VII low-melting agarose in 10% RPMI at a density of 5 × 10^3 cells per well. These cell suspensions were then plated on a layer of 0.9% type VII low-melting agarose in 10% RPMI in 6-well plates and cultured at 37 °C with 5% CO_2. After 2 weeks, colonies were counted, and images were captured at 5× magnification.

Lactate measurement

The media were assayed for lactate levels using a Biosen C-Line analyzer according to the manufacturer's instructions.

Assessing cellular respiration in vitro

In vitro cellular respiration was measured by assessing the oxygen flux of proliferating A549 cells and those undergoing differentiation using a RESIPHER device from Lucid Scientific. A 32-sensor lid compatible with a 96-well plate was utilized for this purpose. IκBα-WT, IκBα-MTS, or control A549 cells were seeded at a density of 10^4 cells per well. Oxygen consumption data were sampled every 3 minutes throughout the experiment.

Statistical analysis

Data are presented as mean ± SEM. Statistical significance was determined using Student's t-test or one-way or two-way analysis of variance (ANOVA), as appropriate, followed by Fisher's least significant difference (LSD) or Bonferroni post hoc tests. The specific statistical tests used and the exact sample size (n) for each experiment are

ARTICLE IN PRESS

indicated in the corresponding figure legends. A P value < 0.05 was considered statistically significant (P ≤ 0.05; P ≤ 0.01; *P ≤ 0.001; **P ≤ 0.0001). All statistical analyses were performed using GraphPad Prism 9.

Further details on materials and methods can be found in the supplementary section.

RESULTS

Mitochondrial targeting reveals a stable IκBα fraction.

We previously reported that reduced IκBα expression in a cohort of lung cancer patients initially impairs tumor growth while inducing mitochondrial dysfunction [18]. Although our initial focus was on patients with low IκBα expression associated with enhanced chemosensitivity, a substantial subset of cases from the same cohort exhibited elevated IκBα levels [18].

To better understand the role of IκBα overexpression, we performed subcellular fractionation of A549 lung cancer cells, and validated fraction purity using cytoplasmic and mitochondrial markers, confirming a strong enrichment. A549 cells were selected as they show elevated IκBα levels, allowing us to reveal the presence of IκBα and other pathway components within the mitochondria (Fig. 1A). Furthermore, data obtained with super-resolution microscopy confirmed IκBα localization inside mitochondria (Fig- 1B). The Pearson correlation coefficient indicates a colocalization between IκBα and the mitochondrial compartment (Fig. 1C). Quantitative analysis of IκBα volume and the volume ratio between the mitochondrial and cytoplasmic compartments further supports this observation (Fig. 1D-1E). Finally, colocalization between IκBα and mitochondrial markers was quantitatively evaluated using the Manders overlap coefficient confirming a statistically significant association of IκBα with mitochondria, supporting its mitochondrial localization (Fig. 1F-G).

To explore the functional role of the mitochondrial IκBα/NF-κB axis, we engineered a fusion protein with a mitochondrial targeting signal (MTS) (residues 1-40 of the amino acid sequence of very long-chain acyl-CoA dehydrogenase)[27] at the N-terminus of IκBα. This construct was expressed generating a lentiviral vector, hereafter referred to as IκBα-MTS (Figure S1a, Supporting Information).

ARTICLE IN PRESS

The latter consistently exhibited exclusive IκBα mitochondrial expression, as evidenced by fluorescence microscopy imaging (Fig. S1A, Supporting Information). Confocal imaging revealed distinct localizations of our construct, demonstrating the presence of wild-type IκBα (IκBα-WT) in different cellular compartments, while IκBα-MTS was localized exclusively to the mitochondria (Fig. S1B, Supporting Information). Additionally, unlike IκBα-WT and endogenous IκBα, IκBα-MTS displayed significant stability following TNFα stimulation (Fig. S1C, Supporting Information). While both IκBα-WT and IκBα-MTS underwent phosphorylation, only the former was degraded (Fig. S1C, Supporting Information). This observation is consistent with the absence of canonical ubiquitin-proteasome activity within the mitochondrial compartment [28–30], which limits proteasomal degradation of mitochondrially targeted IκBα and thereby accounts for the increased stability of the MTS construct. Multiple published studies have underscored the presence of a phosphorylated form of IκBα [31] that remains stable, indicating the existence of an intracellular pool of IκBα resistant to degradation. This suggests its potential sequestration within organelles, such as mitochondria, where proteasome activity is diminished.

Mitochondrial IκBα overexpression enhances the aggressiveness of lung cancer cells.

To assess the impact of mitochondrial IκBα on lung cancer aggressiveness, we overexpressed it in A549 and H460 lung cancer cell lines, with or without p65 silencing, in order to determine the role of NF-κB (Fig. 2A and Fig. S2A, Supporting Information). The overexpression of both IκBα -WT and -MTS resulted in increased cell growth (Fig. 2A, lower panel and Fig. S2B, Supporting Information) and colony formation (Figure 2B). IκBα-WT cells displayed a similar trend, though less pronounced, suggesting that efficient mitochondrial accumulation, achieved *via* the MTS signal, maximizes this proliferative advantage. Notably, the silencing of p65 rescued both phenomena observed in IκBα-WT and IκBα-MTS-constructs, indicating that canonical NF-κB components partially contribute to the proliferative phenotype. Consistent with our prior findings, the overexpression of IκBα-WT and -MTS also led to a reduced sensitivity to apoptosis induced by cisplatin treatment (Fig. 2C).

To investigate the impact of mitochondrial IκBα on the pro-metastatic behavior of lung cancer cells, we compared the phenotypic outcomes of IκBα-WT cells versus IκBα-

ARTICLE IN PRESS

ARTICLE IN PRESS

MTS. Functional assays revealed that the expression of IκBα-MTS significantly enhanced cell motility and invasive capacity, hallmark traits of metastatic potential. In contrast, cells expressing IκBα-WT exhibited no notable changes in migration or invasion compared to controls (Fig. 2D, 2E and Fig. S2C and S2D, Supporting Information). These findings suggest that the subcellular localization of IκBα plays a critical role in modulating metastatic behavior, with mitochondrial IκBα acting as a specific driver of invasive phenotypes in lung cancer cells. In this context, p65 silencing appears insufficient to significantly rescue the phenotype.

Mitochondrial IκBα favors metastatic spread and pro-coagulant state of TME.

Consistent with our *in vitro* findings, tail-vein injection of A549 cells into NSG mice revealed that while IκBα-WT cells showed no significant increase in lung metastasis, cells expressing mitochondrial IκBα-MTS exhibited significantly greater metastatic potential compared to both control and IκBα-WT cells (Fig. 3A).

The pro-metastatic effect of mitochondrial IκBα localization was further validated using a spontaneous metastasis assay. Nude mice were subjected to subcutaneous injections of IκBα-WT, IκBα-MTS, or control A549 cells. 24 days post-engraftment, tumors were surgically resected and analyzed, and mice were euthanized 30 days later (Fig. 3B, upper panel). Consistent with the *in vitro* data, both IκBα -WT and -MTS expression promoted an increase in primary tumor growth and size (Fig. 3B lower panel and 3C). However, concerning lung metastasis formation, an increase was observed exclusively in mice injected with IκBα-MTS-overexpressing lung cancer cells (Fig. 3D). These data, consistent with our previous observations (Fig. 2D and 2E), suggest a role for IκBα in promoting lung cancer aggressiveness. In particular, while IκBα-WT overexpression is insufficient to induce a pro-metastatic phenotype, mitochondrial IκBα may promote metastasis. Intriguingly, only mice injected with IκBα-MTS cells displayed increased blood clot formation in vessels around the metastatic sites (Fig. 3E). Tumors obtained from both IκBα-WT- and IκBα-MTS cells displayed more intense staining for the endothelial cells (ECs) marker CD31, along with atypical vessel structures compared to the A549 control-mice, but the distribution of the pro-hemostasis protein vWF within the vessels differed between the two IκBα-expressing cell lines (Fig. 3F). While in the IκBα-WT expressing tumors, vWF exhibited its typical staining pattern exclusively localized in the vessel wall, IκBα-MTS tumor tissue

ARTICLE IN PRESS

ARTICLE IN PRESS

showed a notable increase in intravascular vWF abundance (Fig. 3F). Given the known effects of the thrombotic cascade on metastasis formation [32–34], this could explain the increased invasiveness of IκBα-MTS A549 cells compared to their IκBα-WT counterparts.

ECs synthesize and release vWF into the bloodstream [35]. To assess how mitochondrial IκBα-expressing lung cancer cells influence endothelial behavior, we exposed human umbilical vein endothelial cells (HUVECs) to tumor-conditioned medium (CM), simulating tumor–endothelium crosstalk *in vitro*. Interestingly, CM from IκBα-MTS expressing cells induced a rapid production of vWF by HUVECs, as indicated by immunofluorescence analysis (Fig. 3G), along with an increase in its mRNA expression (Fig. 3H).

Mitochondrial IκBα triggers ECs activation.

ECs represent the initial barrier that prevents cancer cells from entering the bloodstream and reaching distant sites [36]. Hence, we investigated the functional interconnection between lung cancer cells and ECs. IκBα-MTS cells adhered significantly more to an HUVEC monolayer compared to the control and IκBα-WT lung cancer cell lines (Fig. 4A), while no differences in adhesion were detected in the absence of ECs (Fig. 4B). On the other hand, transmigration experiments revealed the capability of lung cancer cells overexpressing IκBα-MTS to migrate across ECs (Fig. 4C). Moreover, CM derived from IκBα-MTS cells significantly enhanced vessel sprouting and tube formation, suggesting a critical role in angiogenesis and vascular network development (Fig. 4D, Fig. S3A and S3B, Supporting Information). These changes were significantly less prominent with CM from IκBα-WT cells, indicating that these functions are predominantly linked to the mitochondrial localization of IκBα, as previously shown.

To further investigate the crosstalk between lung cancer cells and ECs, we assessed the ability of IκBα engineered lung cancer cells to induce the activation of HUVECs by triggering the expression of adhesion proteins on the EC surface. Upon treating HUVECs with CM from IκBα-expressing cells, qRT-PCR analysis revealed increased expression of RNAs encoding adhesion markers, such as VCAM1, ICAM1, and SELE (Fig. 4E). In line with our previous observation, we showed a significant increase in

ARTICLE IN PRESS

ARTICLE IN PRESS

adhesion of parental A549 cells to HUVECs following treatment with IκBα-MTS CM (Fig. 4F, left and right panels).

To confirm these data *in vivo*, we preconditioned mice by intravenously injecting them with CM from cells expressing IκBα every two days for 24 days (Fig. 4G, upper panel), followed by intravenous injection of parental A549 cells. Notably, mice receiving CM derived from IκBα-MTS cancer cells developed significantly more metastases compared to mice treated with IκBα-WT or parental A549 CM (Fig. 4G, lower panel). These data suggest that lung cancer cells overexpressing IκBα in the mitochondria can alter the premetastatic niche (PMN) through the secretion of extracellular factors.

Mitochondrial IκBα induces metabolic reprogramming in lung cancer cells.

The behavior of neighboring cells is affected by changes in the tumor microenvironment, which in turn is shaped by alterations in cancer cell metabolism [37,38]. To assess potential metabolic changes in engineered lung cancer cells that could impact ECs, we conducted experiments to measure the rate of glucose uptake and catabolism by exploiting the radioactive [H3] glucose assay. After a 2-hour incubation period, the medium was collected, and the radioactivity was measured. As shown in Figure 5A, engineered cells exhibited an increase in glucose uptake and catabolism. In agreement with this observation, IκBα-overexpressing A549 cells, when subjected to measurements of oxygen consumption overtime, showed reduced respiration (Fig. 5B); however, only cells expressing the mitochondrial IκBα exhibited a significant increase in lactate release into the medium (Fig. 5C).

Importantly, the TME is often characterized by acidic conditions due to increased lactate production resulting from enhanced glycolysis [8]. Lactate serves as a signaling molecule, stabilizing pathways such as HIF (Hypoxia-Inducible Factor), which regulate angiogenesis-related gene expression. It also stimulates EC functions crucial for angiogenesis, including proliferation, migration, and tube formation [8]. Recent studies have highlighted the role of lactate in modulating EC behavior, including the release of vWF [39,40]. Consistent with these findings, treatment of HUVECs with 10 mM lactate for 15 minutes resulted in an increase in endothelial adhesion markers and vWF, as shown in Figure 5D and E.

ARTICLE IN PRESS

To illustrate the involvement of glycolytic metabolism in EC activation, we conducted an experiment using acute exposure (4 hours) to 2-deoxy-D-glucose (2DG), a glucose analog that selectively targets glucose metabolism while limiting secondary cellular stress. Pretreating engineered A549 cells with 2DG reduced the levels of pro-adhesive and pro-thrombotic molecules in ECs exposed to their conditioned medium. As shown in Fig. 5F-I, CM derived from IκBα-MTS lung cancer cells significantly reduced the expression of adhesion markers (Fig. 5F-H) and vWF accumulation (Fig.5I). This metabolic change in lung cancer cells, induced by IκBα-MTS overexpression, could explain EC activation and potentially the ability of cancer cells to facilitate the formation of the metastatic niche [41–43].

DISCUSSION

Our study sheds new light on the intricate connection between mitochondrial IκBα, lung cancer cell metabolism, and its profound impact on the TME, particularly affecting ECs and CAT [44,45]. Previous research has established the multifaceted role of IκBα/NF-κB in modulating redox homeostasis in lung cancer cells. Expanding upon this knowledge, our findings revealed distinct phenotypes in lung cancer cells depending on varying expression levels and subcellular localization of the IκBα protein [18].

Unlike in the cytoplasm, where IκBα undergoes rapid degradation following Ser32-Ser36 phosphorylation, mitochondrial IκBα appears resistant to this degradation, allowing for its accumulation. This suggests that overexpressed IκBα, when accumulated in mitochondria, may acquire novel biological functions separate from its canonical role in cytoplasmic NF-κB inhibition. Indeed, mitochondrial IκBα functions appear entirely distinct from its well-known cytoplasmic role in controlling p65/NF-κB activity. Instead, within the mitochondria, IκBα seems to adopt an oncogenic role, significantly boosting the metastatic potential of lung cancer cells. This enhanced metastatic capacity could stem from an increase in circulating tumor cells or more efficient early lung metastasis formation. This interpretation aligns with our *in vitro* RELA-silencing experiments, in which proliferative defects are rescued whereas metastatic behavior is not fully reversed, suggesting that mitochondrial IκBα mediates biological functions beyond canonical NF-κB regulation, potentially through alternative molecular partners.

ARTICLE IN PRESS

ARTICLE IN PRESS

Furthermore, the tumor resection process may have initiated a wound healing response [46], promoting a pro-inflammatory environment favorable to the proliferation and dissemination of cancer cells, particularly those with heightened metastatic potential, such as IκBα-MTS cells. This consideration acquires further relevance within the framework of an inflammatory response, which may be linked to coagulation phenomena triggered by the release of vWF and the formation of microthrombi. These features were notably accentuated in IκBα-MTS primary tumors and metastases. This observation suggests the need for a closer examination of the development of CAT, which poses significant risks for cancer patients [47]. The intricate interplay between CAT and metastasis encompasses various interconnected mechanisms: a hypercoagulable state due to the release of procoagulant factors [48]; platelet activation facilitating tumor cell adhesion and protection [49,50]; enhanced angiogenesis; interaction with the coagulation system promoting tumor growth; and inflammatory responses contributing to thrombosis through cytokine-mediated pathways [51]. Moreover, endothelial dysfunction further exacerbates thrombus formation, facilitating cancer cell extravasation and metastasis formation [52].

Our data suggest that mitochondrial IκBα contributes to metabolic reprogramming, with aerobic glycolysis, and particularly lactate, being a central player in aggressiveness. Indeed, IκBα-MTS cells showed significantly increased extracellular lactate accumulation. This finding suggests alterations in lactate handling rather than glycolytic engagement *per se*, potentially involving differences in lactate export through monocarboxylate transporters (e.g., MCT1/MCT4), changes in pyruvate flux, or mitochondrial activity influencing the balance between lactate production and oxidative metabolism. Addressing these possibilities will require targeted approaches, including MCT inhibition, direct comparisons between lactic acid and sodium lactate, and controlled buffering strategies, which will be essential to disentangle lactate transport-dependent versus pH-driven mechanisms and to further define the metabolic role of mitochondrial IκBα[53].

Notably, lactate release is not only linked to endothelial activation and angiogenesis but also plays a key role in inducing platelet aggregation and enhancing pro-thrombotic activity [54]. While our findings provide strong evidence for lactate as a key signaling molecule driving endothelial activation and the prothrombotic state, we do not exclude the possibility that other secreted metabolites, resulting from the observed mitochondrial dysfunction, could act in concert to shape the pro-metastatic niche.

ARTICLE IN PRESS

Further metabolomic studies could clarify the full spectrum of factors involved in this crosstalk [55].

A key question arising from our study is the direct molecular mechanism by which mitochondrial IκBα impairs oxidative phosphorylation. Identifying its specific binding partners within the mitochondrial proteome is therefore a critical future endeavor to fully elucidate how it triggers metabolic rewiring. One possibility is that IκBα interacts with components of the electron transport chain, mitochondrial metabolic enzymes, or other resident mitochondrial proteins, thereby altering their activity or assembly rather than their expression. Alternatively, mitochondrial IκBα may modulate mitochondrial signaling pathways or protein-protein interactions that indirectly affect respiratory efficiency. These possibilities remain to be experimentally addressed.

It is well established that primary tumors can prime the PMN to facilitate the colonization of disseminated cancer cells, yet the mechanisms by which dormant vasculature is activated at distant sites remain poorly defined. In this context, we investigated the ability of IκBα-MTS-expressing lung cancer cells to modulate ECs and potentially initiate vascular activation in secondary sites, thereby contributing to metastasis formation.

Our findings indicate that mitochondrial IκBα in lung cancer cells disrupts EC homeostasis. Through paracrine signaling, mitochondrial IκBα primary tumors exert influence over distant organs, promoting vascular remodeling and preparing a permissive PMN for circulating cancer cells. These processes collectively enhance lung cancer cell intravasation and metastasis.

Nevertheless, several aspects of this pathway remain to be elucidated. For instance, the mechanism by which IκBα enters the mitochondria warrants further investigation. It is possible that its mitochondrial translocation is mediated by hypoxia and STAT3 signaling pathways [56]. Additionally, recent findings have identified irregularities in MTS sequences [57], suggesting the potential for alternative splicing or mutations affecting IκBα localization.

Importantly, under What is clear, however, is that, under certain specific conditions, particularly e.g. in oncogenic [58] or hypoxic environments [56], IκBα can localize to the mitochondria. Our data suggest a dual role for mitochondrial IκBα. While its effects on

ARTICLE IN PRESS

ARTICLE IN PRESS

cell proliferation and colony formation appear to remain dependent on the p65/NF-κB axis, as indicated by our p65 silencing experiments, the profound metabolic shift towards glycolysis and the subsequent activation of the endothelium appear to be direct consequences of its mitochondrial localization, representing a novel, non-canonical function. Thus, mitochondrial IκBα may contribute to cancer progression through both NF-κB-dependent and independent mechanisms, potentially conferring gain-of-function properties that promote tumor growth and metastasis [59].

Altogether, our findings suggest that mitochondrial localization of IκBα may significantly contribute to the metastatic burden in lung cancer. While RELA silencing provided important insight into pathway dependency, more refined NF-κB functional assays will be necessary to fully delineate canonical versus non-canonical contributions. Importantly, we did not directly quantify NF-κB transcriptional activity in this study; future reporter-based or transcriptomic approaches will be necessary to more precisely define the canonical versus non-canonical contributions to the phenotypes associated with mitochondrial IκBα. Furthermore, as IκBα is a canonical inhibitor of NF-κB, the mitochondrially targeted form used here does not directly engage the cytoplasmic NF-κB regulatory cycle, and therefore its biological effects cannot be interpreted as simple NF-κB inhibition. These limitations outline important avenues for future investigation to disentangle mitochondrial and cytoplasmatic IκBα. Finally, an important limitation of the study is the reliance on overexpression systems to manipulate mitochondrial IκBα localization. Tools to selectively regulate mitochondrial import of endogenous IκBα are not currently available, and future models will be required to confirm these findings under physiological conditions.

ARTICLE IN PRESS

Nonetheless, our findings collectively reveal a potential novel function of IκBα that operates independently of canonical NF-κB signaling. This non-canonical, mitochondria-associated activity may bypass compensatory inhibitory pathways and highlights new therapeutic opportunities aimed at the mitochondrial pool of IκBα or its downstream metabolic and thrombotic effectors.

Abbreviations:

LC-Lung cancer

ECs- Endothelial cells

IκBα -Inhibitor of κB alpha

ARTICLE IN PRESS

TNFα -Tumor necrosis factor alpha

MTS- Mitochondrial targeting signal

IκBα-WT -Wild-type IκBα

ROS-Reactive oxygen species

OXPHOS-Oxidative phosphorylation

ETC-Electron transport chain

OMM-Outer mitochondrial membrane

vWF-Von Willebrand factor

HUVECs-Human umbilical vein endothelial cells

TME-Tumor microenvironment

CM-Conditioned medium

PMN-pre-metastatic niche

CAT-Cancer-associated thrombosis

VCAM1-Vascular cell adhesion molecule 1

ICAM1-Intercellular adhesion molecule 1

SELE -Selectin E

H&E -Hematoxylin and eosin

2DG -2-deoxy-D-glucose

Acknowledgements

This research was supported by Giovani Ricercatori-GR-2021-12374957. GC is supported by Giovani Ricercatori-GR-2021-12374957. GC was supported by FIRC/AIRC Fellowships (Grants no. 25254), AIRC Short-Term Fellowships, and FEBS Short-Term Fellowship. The research leading to these results has received funding from AIRC under IG 2025 - ID. 32647 project – P.I. Morotti Alessandro. Alessio Menga is supported by MFAG ID 25908. JP is supported by 22HLT06 GenomeMET project (European Partnership on Metrology, co-financed by the European Union’s Horizon Europe Research and Innovation Programme and by the Participating States). FO is partially supported by the Italian Ministry of University and Research (MUR) Program “Department of Excellence 2023-2027”, AGING Project - Department of Translational Medicine, University del Piemonte Orientale. MB is supported by the Italian Association for Cancer Research (AIRC IG24930). Porporato Paolo Ettore is supported from AIRC under MFAG 2018 -ID. 21564 project. We extend our sincere thanks to Professor Valeria Poli for her valuable insights and feedback.

ARTICLE IN PRESS

ARTICLE IN PRESS

Conflict of Interest

The authors declare no conflict of interest.

Data availability

All data generated or analyzed during this study are included in this published article and its supplementary information and are available from the corresponding author on reasonable request.

Ethics approval and consent to participate

All methods were performed in accordance with the relevant guidelines and regulations. Animal experiments were conducted in compliance with Animal Welfare Protocol No. 219/2023-PR (ref. CC652.196), as approved by the competent Ethics Committee.

Author contributions

GC and AM conceptualized the work. GC wrote the paper. AM, JP, LA, MB, FO, PEP, IB and MM edited the paper. AB helped with platelets experiments. GC and PP made the figures. GC handled the final edits and submission. DA contributed by assisting with the confocal imaging and creating the graphical abstract. LA, AMenga, and RB assisted with the mouse experiments. AS, CD, MC, CRD, MM, CR, PEP, AMenga and FC assisted with the metabolism experiments. LT helps with super microscopy analysis. AS, MCC and CD help with the revision. The authors read and approved the final manuscript.

ARTICLE IN PRESS

References

1 Gerstberger S, Jiang Q, Ganesh K. Metastasis. *Cell* 2023; **186**: 1564–1579.

2 Jehanno C, Vulin M, Richina V, Richina F, Bentires-Alj M. Phenotypic plasticity during metastatic colonization. *Trends Cell Biol* 2022; **32**: 854–867.

3 Liu Z, Chen J, Ren Y, Liu S, Ba Y, Zuo A *et al.* Multi-stage mechanisms of tumor metastasis and therapeutic strategies. *Signal Transduct Target Ther* 2024; **9**: 270.

ARTICLE IN PRESS

4 Peinado H, Zhang H, Matei IR, Costa-Silva B, Hoshino A, Rodrigues G *et al.* Pre-metastatic niches: organ-specific homes for metastases. *Nat Rev Cancer* 2017; **17**: 302–317.

5 Massagué J, Obenauf AC. Metastatic colonization by circulating tumour cells. *Nature* 2016; **529**: 298–306.

6 Li X, Yang Y, Zhang B, Lin X, Fu X, An Y *et al.* Lactate metabolism in human health and disease. *Signal Transduct Target Ther* 2022; **7**: 305.

7 Gu X-Y, Yang J-L, Lai R, Zhou Z-J, Tang D, Hu L *et al.* Impact of lactate on immune cell function in the tumor microenvironment: mechanisms and therapeutic perspectives. *Front Immunol* 2025; **16**: 1563303.

8 Li Z, Wang Q, Huang X, Yang M, Zhou S, Li Z *et al.* Lactate in the tumor microenvironment: A rising star for targeted tumor therapy. *Front Nutr* 2023; **10**: 1113739.

9 Fernandes CJ, Morinaga LTK, Alves JL, Castro MA, Calderaro D, Jardim CVP *et al.* Cancer-associated thrombosis: the when, how and why. *Eur Respir Rev Off J Eur Respir Soc* 2019; **28**: 180119.

10 Wan T, Song J, Zhu D. Cancer-associated venous thromboembolism: a comprehensive review. *Thromb J* 2025; **23**: 35.

11 Galmiche A, Rak J, Roumenina LT, Saidak Z. Coagulome and the tumor microenvironment: an actionable interplay. *Trends Cancer* 2022; **8**: 369–383.

12 Perkins ND. The diverse and complex roles of NF-κB subunits in cancer. *Nat Rev Cancer* 2012; **12**: 121–132.

ARTICLE IN PRESS

ARTICLE IN PRESS

13 Liu T, Zhang L, Joo D, Sun S-C. NF-κB signaling in inflammation. *Signal Transduct Target Ther* 2017; **2**: 17023-.

14 Courtois G, Gilmore TD. Mutations in the NF-kappaB signaling pathway: implications for human disease. *Oncogene* 2006; **25**: 6831–6843.

15 Hayden MS, Ghosh S. NF-κB in immunobiology. *Cell Res* 2011; **21**: 223–244.

16 Carrà G, Avalle L, Seclì L, Brancaccio M, Morotti A. Shedding Light on NF-κB Functions in Cellular Organelles. *Front Cell Dev Biol* 2022; **10**: 841646.

17 Karin M, Delhase M. The I kappa B kinase (IKK) and NF-kappa B: key elements of proinflammatory signalling. *Semin Immunol* 2000; **12**: 85–98.

18 Carrà G, Ermondi G, Riganti C, Righi L, Caron G, Menga A *et al.* IκBα targeting promotes oxidative stress-dependent cell death. *J Exp Clin Cancer Res CR* 2021; **40**: 136.

19 Chew HK, Wun T, Harvey D, Zhou H, White RH. Incidence of venous thromboembolism and its effect on survival among patients with common cancers. *Arch Intern Med* 2006; **166**: 458–464.

20 Kuderer NM, Ortel TL, Francis CW. Impact of venous thromboembolism and anticoagulation on cancer and cancer survival. *J Clin Oncol Off J Am Soc Clin Oncol* 2009; **27**: 4902–4911.

21 Mojzisch A, Brehm MA. The Manifold Cellular Functions of von Willebrand Factor. *Cells* 2021; **10**: 2351.

ARTICLE IN PRESS

ARTICLE IN PRESS

22 Dhami SPS, Patmore S, Comerford C, Byrne CM, Cavanagh B, Castle J *et al.* Breast cancer cells mediate endothelial cell activation, promoting von Willebrand factor release, tumor adhesion, and transendothelial migration. *J Thromb Haemost JTH* 2022; **20**: 2350–2365.

23 Yang A-J, Wang M, Wang Y, Cai W, Li Q, Zhao T-T *et al.* Cancer cell-derived von Willebrand factor enhanced metastasis of gastric adenocarcinoma. *Oncogenesis* 2018; **7**: 12.

24 Suzuki YJ. Cell signaling pathways for the regulation of GATA4 transcription factor: Implications for cell growth and apoptosis. *Cell Signal* 2011; **23**: 1094–1099.

25 Patmore S, Dhami SPS, O'Sullivan JM. Von Willebrand factor and cancer; metastasis and coagulopathies. *J Thromb Haemost JTH* 2020; **18**: 2444–2456.

26 O'Sullivan JM, Preston RJS, Robson T, O'Donnell JS. Emerging Roles for von Willebrand Factor in Cancer Cell Biology. *Semin Thromb Hemost* 2018; **44**: 159–166.

27 Cogswell PC, Kashatus DF, Keifer JA, Guttridge DC, Reuther JY, Bristow C *et al.* NF-kappa B and I kappa B alpha are found in the mitochondria. Evidence for regulation of mitochondrial gene expression by NF-kappa B. *J Biol Chem* 2003; **278**: 2963–2968.

28 Rödl S, Herrmann JM. The role of the proteasome in mitochondrial protein quality control. *IUBMB Life* 2023; **75**: 868–879.

29 Krämer L, Groh C, Herrmann JM. The proteasome: friend and foe of mitochondrial biogenesis. *FEBS Lett* 2021; **595**: 1223–1238.

ARTICLE IN PRESS

ARTICLE IN PRESS

30 Meul T, Berschneider K, Schmitt S, Mayr CH, Mattner LF, Schiller HB *et al.* Mitochondrial Regulation of the 26S Proteasome. *Cell Rep* 2020; **32**: 108059.

31 Albensi BC. What Is Nuclear Factor Kappa B (NF-κB) Doing in and to the Mitochondrion? *Front Cell Dev Biol* 2019; **7**: 154.

32 Bottero V, Rossi F, Samson M, Mari M, Hofman P, Peyron JF. Ikappa b-alpha, the NF-kappa B inhibitory subunit, interacts with ANT, the mitochondrial ATP/ADP translocator. *J Biol Chem* 2001; **276**: 21317–21324.

33 Johnson RF, Witzel I-I, Perkins ND. p53-dependent regulation of mitochondrial energy production by the RelA subunit of NF-κB. *Cancer Res* 2011; **71**: 5588–5597.

34 Barshad G, Marom S, Cohen T, Mishmar D. Mitochondrial DNA Transcription and Its Regulation: An Evolutionary Perspective. *Trends Genet TIG* 2018; **34**: 682–692.

35 Laforge M, Rodrigues V, Silvestre R, Gautier C, Weil R, Corti O *et al.* NF-κB pathway controls mitochondrial dynamics. *Cell Death Differ* 2016; **23**: 89–98.

36 Fang J, Lu Y, Zheng J, Jiang X, Shen H, Shang X *et al.* Exploring the crosstalk between endothelial cells, immune cells, and immune checkpoints in the tumor microenvironment: new insights and therapeutic implications. *Cell Death Dis* 2023; **14**: 586.

37 Cerezo M, Rocchi S. Cancer cell metabolic reprogramming: a keystone for the response to immunotherapy. *Cell Death Dis* 2020; **11**: 964.

ARTICLE IN PRESS

ARTICLE IN PRESS

38 Falkenberg KD, Rohlenova K, Luo Y, Carmeliet P. The metabolic engine of endothelial cells. *Nat Metab* 2019; **1**: 937–946.

39 Hou Z, Yan W, Li T, Wu W, Cui Y, Zhang X *et al.* Lactic acid-mediated endothelial to mesenchymal transition through TGF-β1 contributes to in-stent stenosis in poly-L-lactic acid stent. *Int J Biol Macromol* 2020; **155**: 1589–1598.

40 Fan M, Yang K, Wang X, Chen L, Gill PS, Ha T *et al.* Lactate promotes endothelial-to-mesenchymal transition via Snail1 lactylation after myocardial infarction. *Sci Adv* 2023; **9**: eadc9465.

41 Liu S, Zhao H, Hu Y, Yan C, Mi Y, Li X *et al.* Lactate promotes metastasis of normoxic colorectal cancer stem cells through PGC-1α-mediated oxidative phosphorylation. *Cell Death Dis* 2022; **13**: 651.

42 Jin M, Cao W, Chen B, Xiong M, Cao G. Tumor-Derived Lactate Creates a Favorable Niche for Tumor via Supplying Energy Source for Tumor and Modulating the Tumor Microenvironment. *Front Cell Dev Biol* 2022; **10**: 808859.

43 Pérez-Tomás R, Pérez-Guillén I. Lactate in the Tumor Microenvironment: An Essential Molecule in Cancer Progression and Treatment. *Cancers* 2020; **12**: 3244.

44 Khorana AA, Mackman N, Falanga A, Pabinger I, Noble S, Ageno W *et al.* Cancer-associated venous thromboembolism. *Nat Rev Dis Primer* 2022; **8**: 11.

45 Noble S, Pasi J. Epidemiology and pathophysiology of cancer-associated thrombosis. *Br J Cancer* 2010; **102**: S2–S9.

ARTICLE IN PRESS

ARTICLE IN PRESS

46 Kong B, Michalski CW, Friess H, Kleeff J. Surgical procedure as an inducer of tumor angiogenesis. *Exp Oncol* 2010; **32**: 186–189.

47 Pavlovic D, Niciforovic D, Markovic M, Papic D. Cancer-Associated Thrombosis: Epidemiology, Pathophysiological Mechanisms, Treatment, and Risk Assessment. *Clin Med Insights Oncol* 2023; **17**: 11795549231220297.

48 Nasser NJ, Fox J, Agbarya A. Potential Mechanisms of Cancer-Related Hypercoagulability. *Cancers* 2020; **12**: 566.

49 Bian X, Yin S, Yang S, Jiang X, Wang J, Zhang M *et al.* Roles of platelets in tumor invasion and metastasis: A review. *Heliyon* 2022; **8**: e12072.

50 Anvari S, Osei E, Maftoon N. Interactions of platelets with circulating tumor cells contribute to cancer metastasis. *Sci Rep* 2021; **11**: 15477.

51 Sharma S, Tyagi T, Antoniak S. Platelet in thrombo-inflammation: Unraveling new therapeutic targets. *Front Immunol* 2022; **13**: 1039843.

52 Preuss SF, Grieshober D, Augustin HG. Systemic Reprogramming of Endothelial Cell Signaling in Metastasis and Cachexia. *Physiol Bethesda Md* 2023; **38**: 0.

53 Chen Z, Han F, Du Y, Shi H, Zhou W. Hypoxic microenvironment in cancer: molecular mechanisms and therapeutic interventions. *Signal Transduct Target Ther* 2023; **8**: 70.

54 Estevez B, Du X. New Concepts and Mechanisms of Platelet Activation Signaling. *Physiol Bethesda Md* 2017; **32**: 162–177.

ARTICLE IN PRESS

55 Ząbczyk M, Natorska J, Janion-Sadowska A, Malinowski KP, Janion M, Undas A. Elevated Lactate Levels in Acute Pulmonary Embolism Are Associated with Prothrombotic Fibrin Clot Properties: Contribution of NETs Formation. *J Clin Med* 2020; **9**: 953.

56 Ivanova IG, Perkins ND. Hypoxia induces rapid, STAT3 and ROS dependent, mitochondrial translocation of RelA(p65) and IκBα. *Biosci Rep* 2019; **39**: BSR20192101.

57 Bykov YS, Flohr T, Boos F, Zung N, Herrmann JM, Schuldiner M. Widespread use of unconventional targeting signals in mitochondrial ribosome proteins. *EMBO J* 2022; **41**: e109519.

58 Pazarentzos E, Mahul-Mellier A-L, Datler C, Chaisaklert W, Hwang M-S, Kroon J *et al.* IκBα inhibits apoptosis at the outer mitochondrial membrane independently of NF-κB retention. *EMBO J* 2014; **33**: 2814–2828.

59 Morotti A, Crivellaro S, Panuzzo C, Carrà G, Guerrasio A, Saglio G. IκB-α: At the crossroad between oncogenic and tumor-suppressive signals. *Oncol Lett* 2017; **13**: 531–534.

ARTICLE IN PRESS

Figure Legends

Figure 1. Mitochondrial targeting reveals a stable IκBα fraction.

(A) Western blot analysis of cytoplasmic and mitochondrial subcellular fractionation of A549 cells, highlighting the presence of IκBα and its associated pathway within the mitochondria. (B) Images of A549 cells captured with the Elyra 7 Structured Illumination Microscope, along with a cropped zoomed-in view. In the images, IκBα is labeled in green, while the mitochondrial marker (mitotracker) is labeled in red. Scale

ARTICLE IN PRESS

bars: main image - 5 μm; zoom in - 1 μm (C) Pearson correlation coefficient analysis was performed to assess the co-localization of IκBα with mitochondria. The results indicate a higher Pearson coefficient for IκBα in the mitochondrial compartment, suggesting localization or enrichment of IκBα within mitochondria in lung cancer cells. (D-E) Volume and volume ratio of IκBα levels in mitochondria compared to the cytoplasmic fraction. (F) Manders overlap coefficient (M1 and M2), indicating the fraction of IκBα signal overlapping with mitochondria and vice versa. Statistical significance of the observed colocalization was assessed by Costes randomization analysis. (G) Image depicting the mitochondrial localization of IκBα.

All panels show endogenous IκBα unless otherwise indicated. Mitochondrial localization analyses were performed on cells expressing endogenous IκBα.

Figure 2. Mitochondrial IκBα overexpression enhances aggressiveness of lung cancer cells.

(A) Upper Panel: Western blot analysis of IκBα and p65 in A549 cells demonstrating the overexpression of WT and MTS variants compared to control cells, along with p65 silencing. Lower Panel: Proliferation was evaluated over 4 days using the CellTiter Glo assay. Graph shows means ± SEM, N=3 independent experiments, P-values are from Student's t-test, with each condition compared to the control cells. $^*P < 0.05$. (B) Colony formation assay, with representative images. Graph shows means ± SEM, N=4 independent experiments. Statistical significance was determined using Student's *t*-test, with WT and MTS conditions compared to control cells. $^{**}P < 0.01$; $^{***}P < 0.001$; (C) Flow cytometry analysis of apoptotic induction following cisplatin treatment for 48 hours. Graph shows means ± SEM, N=4 independent experiments. Statistical significance was determined using Student's *t*-test, with each experimental condition compared to cisplatin-treated control cells. $^*P < 0.05$. (D) Invasion assay, shown as fold change relative to control cells. Representative images of cells that have invaded through the membrane, stained with crystal violet are shown. Graph shows means ± SEM, N=6 independent experiments Statistical significance was determined using Student's *t*-test, with WT and MTS conditions compared to control cells. $^*P < 0.05$; $^{**}P < 0.01$. (E) Left Panel: Fold change of wound closure, illustrating the progressive wound healing at 0 hours and 15 hours post-wounding. Fold change relative to the control condition, normalized to 1. Right Panel: Representative pictures captured at the indicated time points to offer visual insight into the dynamic healing process. Graph

ARTICLE IN PRESS

shows means ± SEM, N=8 independent experiments Statistical significance was determined using Student's *t*-test, with WT and MTS conditions compared to control cells. **P < 0.01. WT and MTS indicate overexpression constructs for wild-type IκBα and mitochondrially targeted IκBα, respectively. "Control" refers to cells expressing endogenous IκBα only. Conditions including "shRELA" denote p65/RELA silencing used to assess NF-κB pathway contribution.

Figure 3. Mitochondrial IκBα favors metastatic spread and pro-coagulant state of TME.

All *in vivo* experiments were performed using A549 cells infected with control, IκBα-WT, or IκBα-MTS overexpression vectors.

(A) Upper Panel: quantification of metastases obtained from the *in vivo* metastasis assay with A549 cells. Lower Panel: Representative images stained with hematoxylin and eosin (H&E) depict metastatic lesions, providing visual representation of metastatic spread *in vivo*. Data are presented as mean ± SEM from N = 10 mice per group. Statistical significance was determined by one-way ANOVA, with WT and IκBα-MTS groups compared to control mice. **P < 0.01. (B) Left Panel: Schematic representation illustrating the workflow of *in vivo* experiment. Nude mice were subcutaneously injected with IκBα -overexpressing A549 cells, after 24 days primary tumors were surgically dissected and mice sacrificed at day 50 to allow lung metastasis analysis. Right panel: tumor growth curve of mice injected with A549 cells infected with control vector, WT, or IκBα- MTS, measured by caliper every 7 days. Data are shown as mean ± SEM from N = 11 mice per group. Statistical significance was determined by one-way ANOVA, with WT and IκBα-MTS groups compared to control mice. **P < 0.01. (C) Tumor weight (grams) measured at the time of resection (day 24 post-injection). Data are shown as mean ± SEM from N = 11 mice per group. (D) Left Panel: Quantification showing the number of metastases observed in the experimental mice 26 days after tumor resection. Statistical significance was determined by two-way ANOVA, assessing the effects of IκBα construct and experimental time point, between WT or IκBα-MTS and control groups. ****P < 0.0001. Right Panel: Representative images of whole lung sections stained with H&E, showing metastatic lesions. (E) Left panel: Representative images stained with H&E illustrate microthrombi formation in lung vessels of mice injected subcutaneously with A549 cells carrying control vector, WT, or MTS IκBα. Right panel: Quantification of microthrombi. Data are shown as mean ± SEM from N = 11 mice per group. Statistical

ARTICLE IN PRESS

significance was determined by two-way ANOVA, with WT and IκBα-MTS groups compared to control mice. **P < 0.01. (F) Immunofluorescence staining was performed on tumor cryosections from A549 cells infected with control vector, WT, or MTS IκBα. DAPI was used to visualize cell nuclei (blue), CD31 for endothelial cells (red), and vWF (green). (G) Left panel: Immunofluorescence analysis of HUVECs treated with conditioned medium (CM) derived from A549 cells infected with control vector, WT, or MTS IκBα for 15 minutes. Right panel: Fold change quantification of vWF signal in HUVECs. Data are presented as mean ± SEM. Statistical significance was determined using Student's t-test, with WT or IκBα-MTS CM compared to control CM. *P < 0.05. (H) Evaluation of vWF mRNA expression in HUVECs Treated with indicated CM for 15 minutes. Graph shows means ± SEM, N=3 independent experiments. Statistical significance was determined using Student's *t*-test, with WT or IκBα-MTS CM compared to control CM. *P < 0.05; **P < 0.01.

Figure 4: Mitochondrial IκBα triggers ECs activation.

(A) Quantification of GFP-expressing A549 cells (Control, WT-IκBα, or MTS-IκBα, with or without p65 silencing) adherent on a HUVEC monolayer, as measured by FACS analysis. Graph shows means ± SEM, N=3 independent experiments. Statistical significance was determined using Student's t-test, with each experimental group compared to the corresponding control cells. **P < 0.01; ***P < 0.001; ****P < 0.0001. (B). Fold change in adhesion of lung cancer cells relative to control, as described in A, on plates. Graph shows means ± SEM, N=3 independent experiments. Statistical significance was determined using Student's *t*-test, with each condition compared to control cells. (C) Left panel: Fold change of lung cancer cells described in A relative to control, illustrating their migratory behavior. Graph shows means ± SEM, N=4 independent experiments. Statistical significance was determined using Student's t-test, with each condition compared to control cells. *P < 0.05. Right panel: Representative images showing GFP+ lung cancer cells transmigrated through a HUVEC monolayer. (D) Measurement of sprout length induced by conditioned medium (CM) derived from the cell lines described in A. Graph shows means ± SEM, N=3 independent experiments Statistical significance was determined using Student's t-test, with each CM treatment compared to control CM. ***P < 0.001; ****P < 0.0001. (E) Quantitative RT-PCR analysis performed on HUVECs treated with CM from A549 cells for 24 hours, which were infected with control vector, WT, or MTS IκBα. Data are

ARTICLE IN PRESS

mean ± SEM from N = 3 independent experiments. Statistical significance was determined using Student's t-test, with each CM condition compared to control CM. *P < 0.05; **P < 0.01. (F) Upper panel: Schematic representation of experimental setup. HUVECs were pre-treated with CM from IκBα overexpressing A549 for 24 hours, then GFP-positive A549 were plated on a HUVEC monolayer to assess their adhesion potential. Lower left panel: Fold change in adherent GFP-positive A549 cells adherent on HUVEC cells after treatment with the indicated CM for 24 hours. Data are mean ± SEM from N = 4 independent experiments. Statistical significance was determined using Student's t-test, with each CM treatment compared to control CM. *P < 0.05. Lower Right panel: Representative images of adherent GFP-positive A549 cells on the HUVECs cell layer. (G) Upper Panel: Schematic representation of experimental setup. Lower Left panel: Quantification of lung metastases in mice preconditioned with the indicated CM prior to injection with parental A549 cells. Data are mean ± SEM from N = 4 mice per group. Statistical significance was determined using one-way ANOVA, with WT or MTS CM–preconditioned mice compared to control CM. *P < 0.05. Lower Right panel: Representative pictures of lungs stained with H&E highlighting metastatic lesions.

"Control" indicates cells expressing endogenous IκBα only. WT and MTS indicate overexpression constructs. Where indicated, "shRELA" denotes RELA/p65 silencing. Conditioned medium (CM) was collected separately from each condition and applied to HUVECs as specified.

ARTICLE IN PRESS

Figure 5: Mitochondrial IκBα induces metabolic reprogramming in lung cancer cells.

Metabolic assays were performed on A549 cells expressing endogenous IκBα (Control), or overexpressing IκBα-WT or IκBα-MTS. In panels where indicated, p65/RELA silencing (shRELA) was used to assess NF-κB dependency.

(A) Quantification of glucose uptake in A549 cells infected with control vector, WT, or MTS IκBα and silenced or not for p65. Cells were incubated with [^{3}H]-glucose for 2 hours. After incubation, medium was collected and radioactivity was measured using liquid scintillation counting, indicating the rate of glucose uptake and utilization by the cells. Data are mean ± SEM from N = 3 independent experiments. Statistical significance was determined by one-way ANOVA, with WT or MTS ± shRELA compared to corresponding control cells. ****P < 0.0001. (B) Oxygen flux of A549 cells described in A measured using the RESIPHER. Data were sampled every 3

ARTICLE IN PRESS

hours to monitor oxygen consumption rates. Data are mean ± SEM from N = 3 independent experiments. Statistical significance was determined by two-way ANOVA, with WT or MTS compared to control cells. ****P < 0.0001. (C) Lactate concentrations in the culture media were measured after 48 hours of incubation of A549 cells infected with control vector, WT, or MTS IκBα. Cells were cultured under normoxic conditions. Lactate release was quantified using Biosen C. Values are mean ± SEM from N = 3 independent experiments. Statistical significance was determined by one-way ANOVA, with WT or MTS compared to control cells. *P < 0.05. (D) Quantitative RT-PCR analysis performed on HUVECs treated with different concentration of lactate for 15 minutes. Data are mean ± SEM from N = 4 independent experiments. Statistical significance was determined by one-way ANOVA compared to untreated HUVECs. ****P < 0.0001. (E) Immunofluorescence analysis of HUVECs treated with 10 mM lactate for 15 minutes. (F-I) Quantitative RT-PCR analysis was conducted on HUVECs exposed to conditioned medium (CM) derived from A549 cells for 24 hours. The A549 cells were infected with control vector, WT, or MTS IκBα, and subsequently treated or untreated with 8 mM 2-deoxyglucose (2DG) for 4 hours prior to collecting the CM. Data are mean ± SEM from N = 8 independent experiments. Statistical significance was determined by one-way ANOVA, with each CM condition compared to control CM. *P < 0.05; **P < 0.01; ***P < 0.001.

ARTICLE IN PRESS

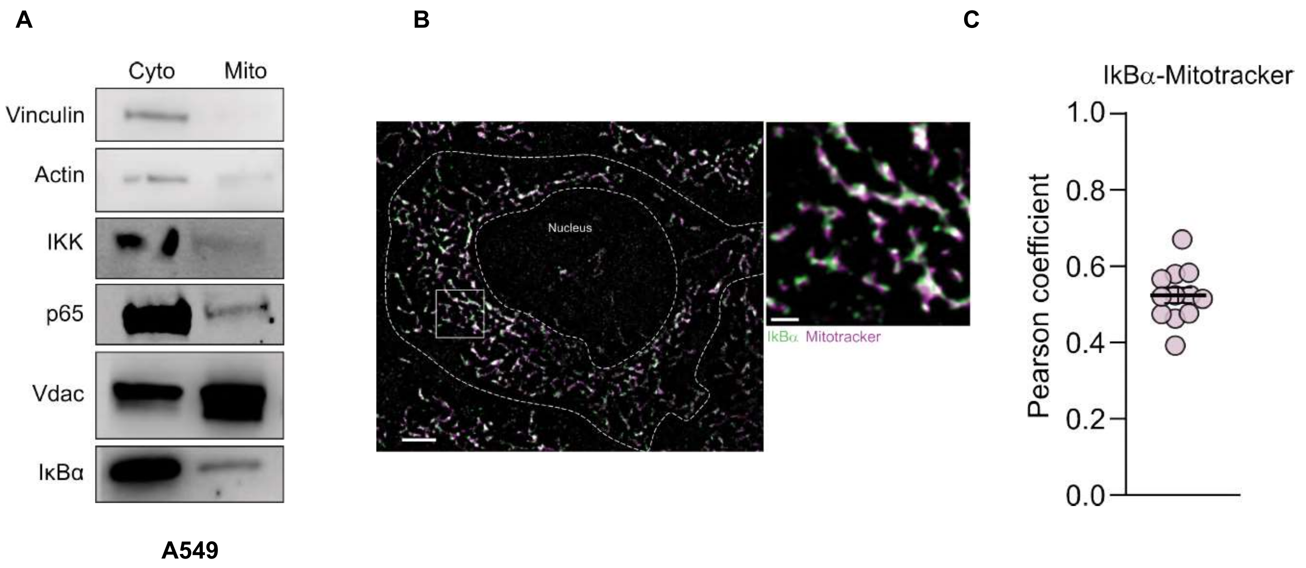
A
Cyto
Mito
Vinculin
Actin
IKK
p65
Vdac
IκBα
A549
B
Nucleus
IkBα Mitotracker
C
IkBα-Mitotracker
Pearson coefficient
1.0
0.8
0.6
0.4
0.2
0.0

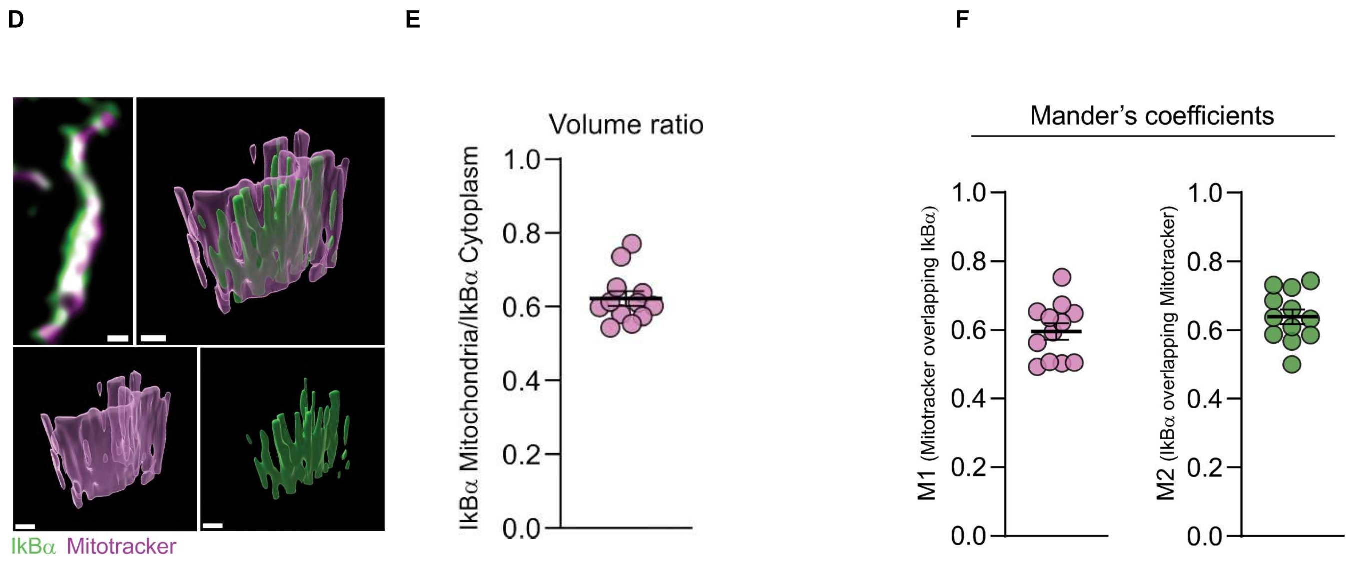
D
IkBα Mitotracker
E
Volume ratio
IkBα Mitochondria/IkBα Cytoplasm
1.0
0.8
0.6
0.4
0.2
0.0
F
Mander's coefficients
M1 (Mitotracker overlapping IkBα)
M2 (IkBα overlapping Mitotracker)
1.0
0.8
0.6
0.4
0.2
0.0

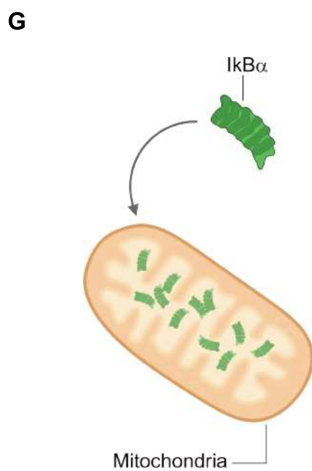
G
IkBα
Mitochondria

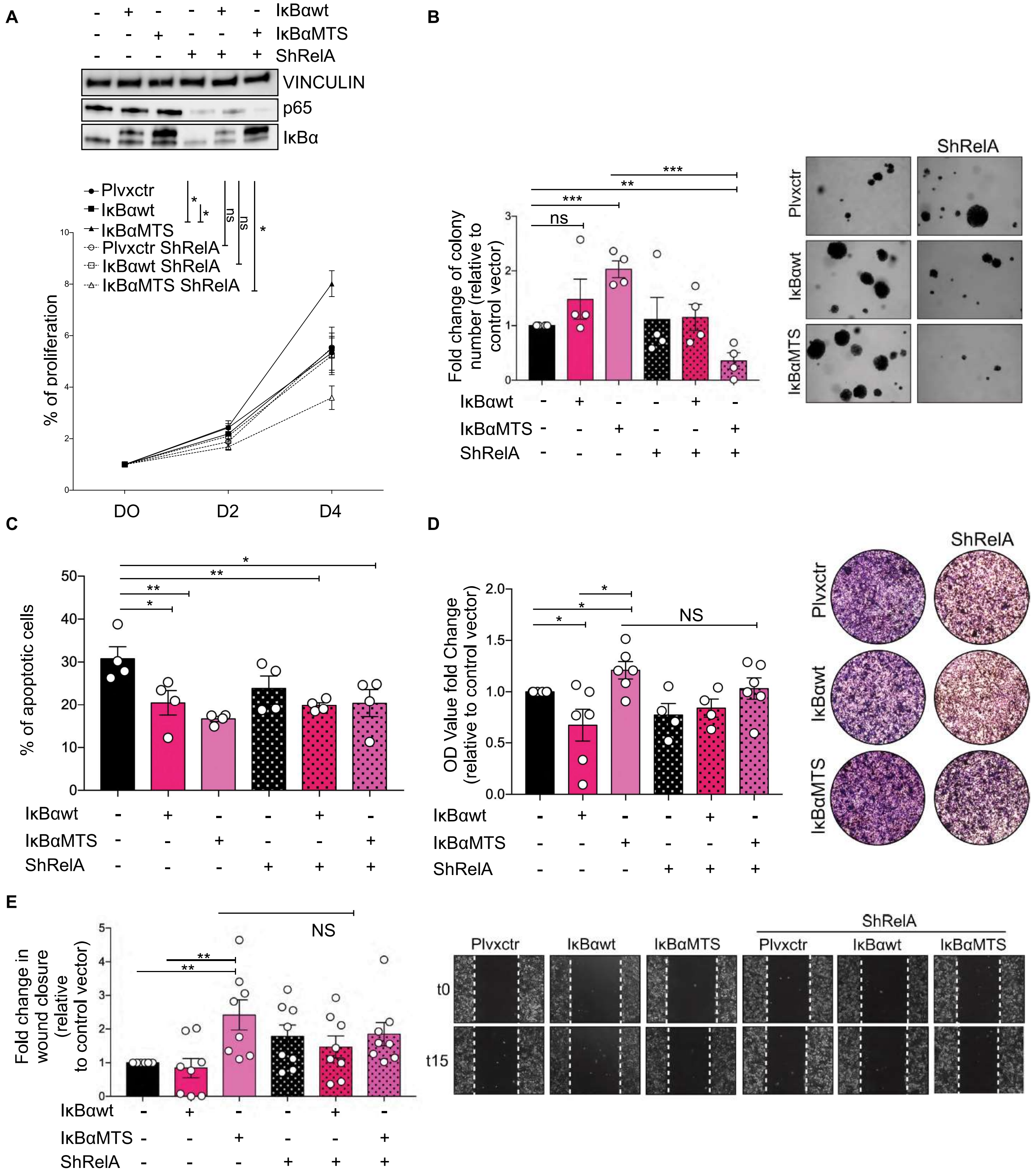
A
IκBαwt
IκBαMTS
ShRelA
VINCULIN
p65
IκBα
Plvxctr
IκBαwt
IκBαMTS
Plvxctr ShRelA
IκBαwt ShRelA
IκBαMTS ShRelA
% of proliferation
DO
D2
D4
B
Fold change of colony number (relative to control vector)
ShRelA
Plvxctr
IκBαwt
IκBαMTS
C
% of apoptotic cells
D
OD Value fold Change (relative to control vector)
NS
E
Fold change in wound closure (relative to control vector)
t0
t15

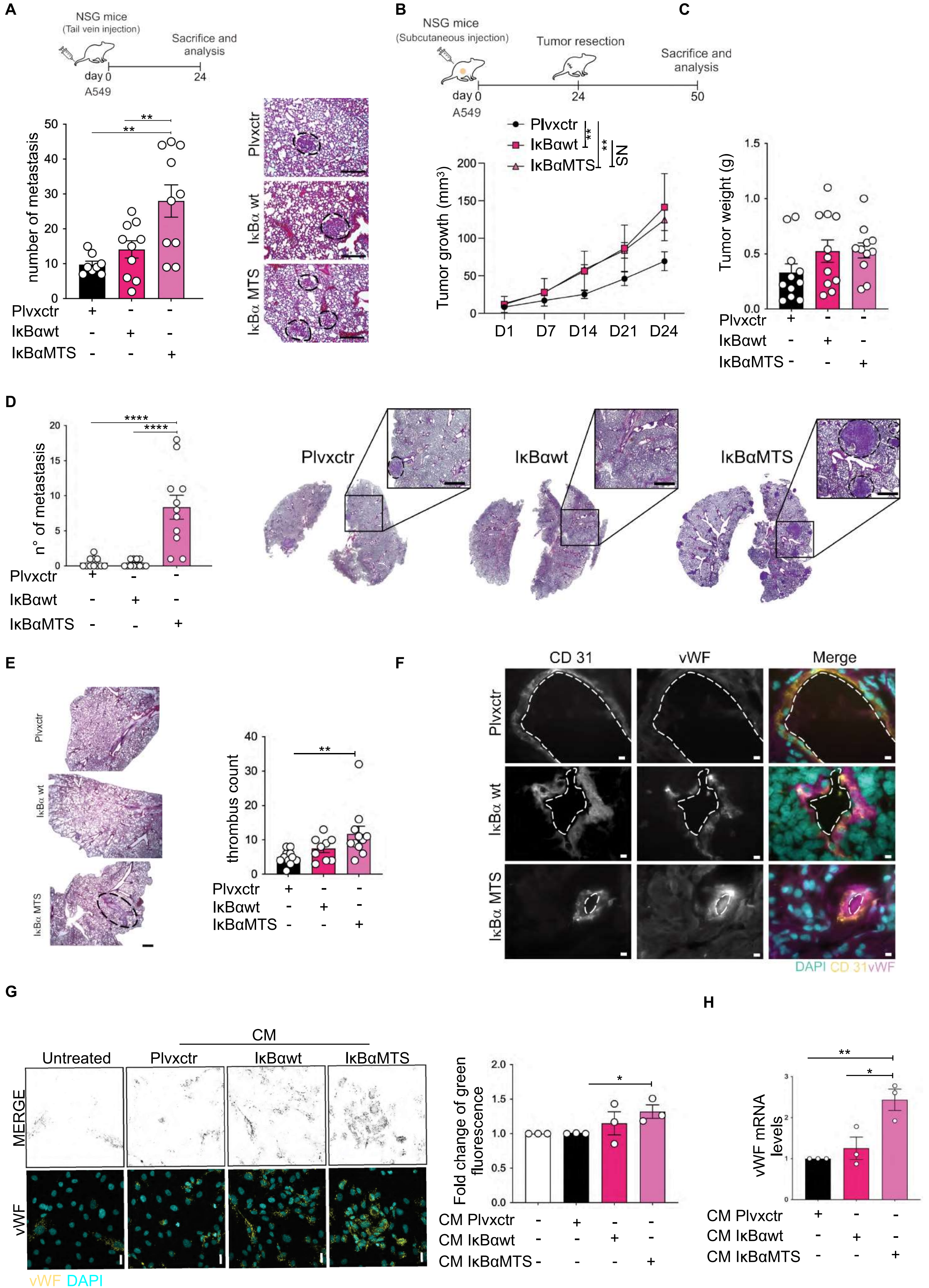
A
NSG mice
(Tail vein injection)
Sacrifice and analysis
day 0
24
A549
number of metastasis
Plvxctr
IκBαwt
IκBαMTS
Plvxctr
IκBα wt
IκBα MTS
B
NSG mice
(Subcutaneous injection)
Tumor resection
Sacrifice and analysis
day 0
24
50
A549
Plvxctr
IκBαwt
IκBαMTS
NS
Tumor growth (mm³)
D1
D7
D14
D21
D24
C
Tumor weight (g)
Plvxctr
IκBαwt
IκBαMTS
D
n° of metastasis
Plvxctr
IκBαwt
IκBαMTS
E
Plvxctr
IκBα wt
IκBα MTS
thrombus count
Plvxctr
IκBαwt
IκBαMTS
F
CD 31
vWF
Merge
Plvxctr
IκBα wt
IκBα MTS
DAPI CD 31vWF
G
CM
Untreated
Plvxctr
IκBαwt
IκBαMTS
MERGE
vWF
vWF DAPI
Fold change of green fluorescence
CM Plvxctr
CM IκBαwt
CM IκBαMTS
H
vWF mRNA levels
CM Plvxctr
CM IκBαwt
CM IκBαMTS

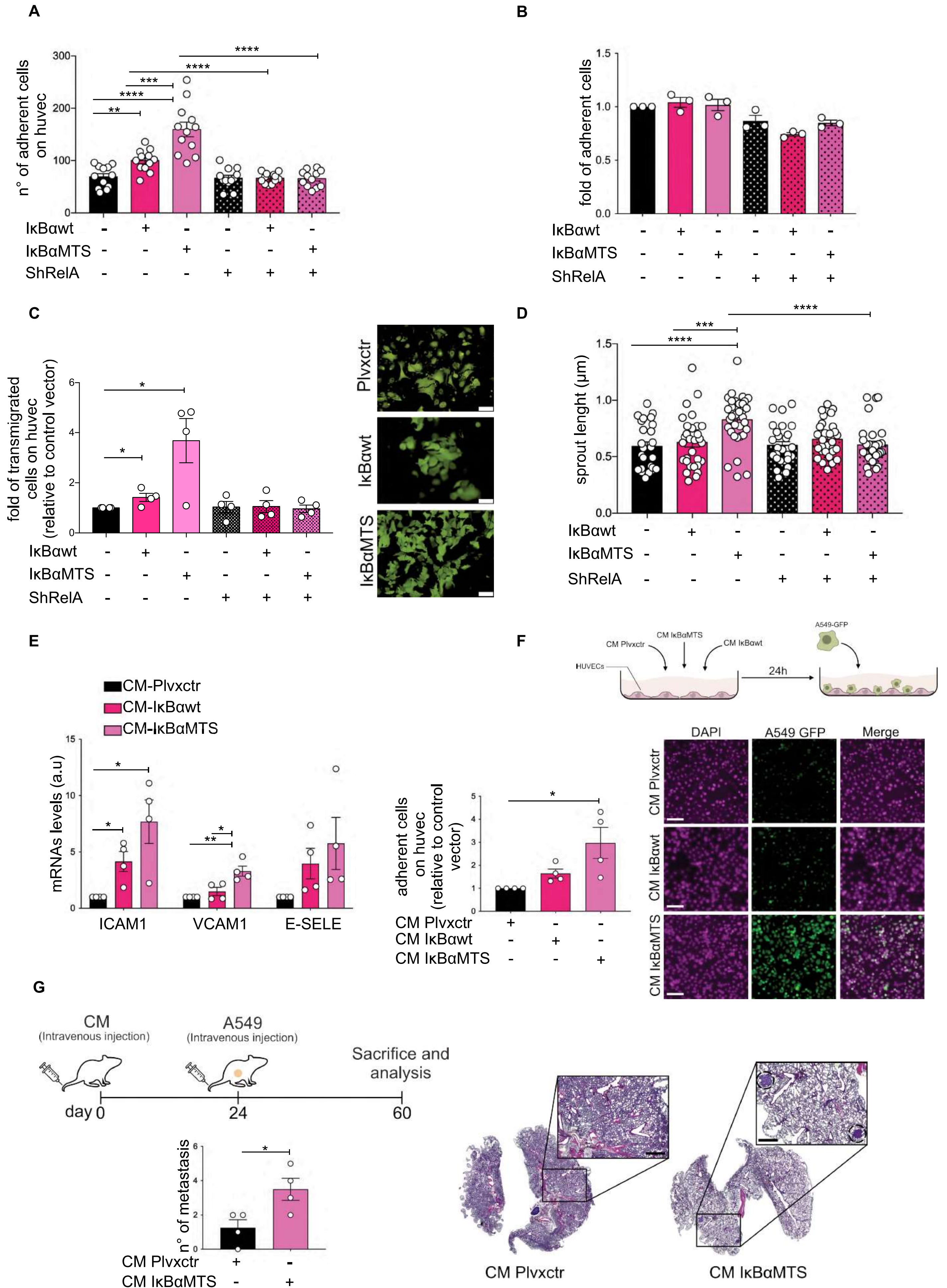

A
n° of adherent cells on huvec
IκBαwt
IκBαMTS
ShRelA
B
fold of adherent cells
C
fold of transmigrated cells on huvec (relative to control vector)
Plvxctr
IκBαwt
IκBαMTS
D
sprout lenght (μm)
E
CM-Plvxctr
CM-IκBαwt
CM-IκBαMTS
mRNAs levels (a.u)
ICAM1
VCAM1
E-SELE
F
CM Plvxctr
CM IκBαMTS
CM IκBαwt
HUVECs
24h
A549-GFP
DAPI
A549 GFP
Merge
adherent cells on huvec (relative to control vector)
G
CM
(Intravenous injection)
A549
(Intravenous injection)
Sacrifice and analysis
day 0
24
60
n° of metastasis
CM Plvxctr
CM IκBαMTS

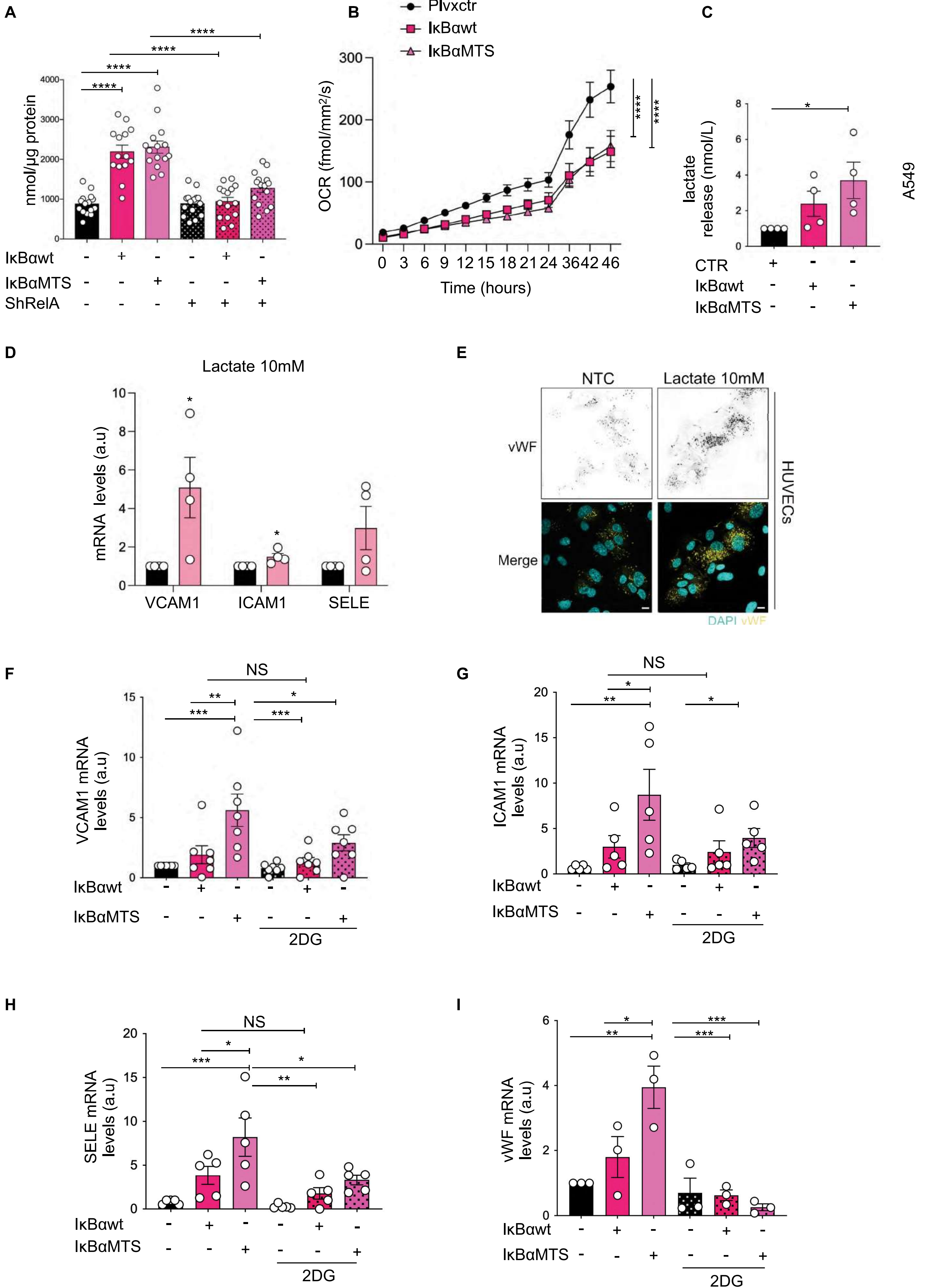

A
nmol/µg protein
IκBαwt
IκBαMTS
ShRelA
B
PIvxctr
IκBαwt
IκBαMTS
OCR (fmol/mm²/s)
Time (hours)
C
lactate release (nmol/L)
CTR
IκBαwt
IκBαMTS
A549
D
Lactate 10mM
mRNA levels (a.u)
VCAM1
ICAM1
SELE
E
NTC
Lactate 10mM
vWF
Merge
HUVECs
DAPI vWF
F
VCAM1 mRNA levels (a.u)
IκBαwt
IκBαMTS
2DG
NS
G
ICAM1 mRNA levels (a.u)
IκBαwt
IκBαMTS
2DG
NS
H
SELE mRNA levels (a.u)
IκBαwt
IκBαMTS
2DG
NS
I
vWF mRNA levels (a.u)
IκBαwt
IκBαMTS
2DG

ARTICLE IN PRESS